

Visualizing single-molecule diffusion in mesoporous materials

Andreas Zürner^{1*}, Johanna Kirstein^{1*}, Markus Döblinger¹, Christoph Bräuchle¹ & Thomas Bein¹

Periodic mesoporous materials formed through the cooperative self-assembly of surfactants and framework building blocks can assume a variety of structures^{1–3}, and their widely tuneable properties make them attractive hosts for numerous applications^{4–7}. Because the molecular movement in the pore system is the most important and defining characteristic of porous materials⁸, it is of interest to learn about this behaviour as a function of local structure. Generally, individual fluorescent dye molecules can be used as molecular beacons with which to explore the structure of—and the dynamics within—these porous hosts^{9–13}, and single-molecule fluorescence techniques provide detailed insights into the dynamics of various processes, ranging from biology^{14,15} to heterogeneous catalysis¹⁶. However, optical microscopy methods cannot directly image the mesoporous structure of the host system accommodating the diffusing molecules, whereas transmission electron microscopy provides detailed images of the porous structure¹⁷, but no dynamic information. It has therefore not been possible to ‘see’ how molecules diffuse in a real nanoscale pore structure. Here we present a combination of electron microscopic mapping and optical single-molecule tracking experiments to reveal how a single luminescent dye molecule travels through linear or strongly curved sections of a mesoporous channel system. In our approach we directly correlate porous structures detected by transmission electron microscopy with the diffusion dynamics of single molecules detected by optical microscopy. This opens up new ways of understanding the interactions of host and guest.

For the implementation of our approach, key sample requirements include extremely thin mesoporous films on electron-transparent substrates, the inclusion of different types of markers, and optical transparency. We spin-coated a solution with a mixture of tetraethyl orthosilicate, Brij 56, HCl, ethanol and water (in a molar ratio of 1:0.144:0.06:61.69:210), resulting in thin films, measured by ellipsometry to be 100 nm thick. The corresponding two-dimensional grazing-incidence small-angle X-ray scattering (2D-GISAXS) pattern shows a two-dimensional hexagonal arrangement of mesoporous silica (Fig. 1a; for details see Methods). Strongly fluorescent terrylene diimide (TDI) molecules^{18,19}, acting as molecular beacons for single-molecule tracking, polystyrene beads (280 nm in diameter) as markers that are visible in both transmission electron microscopy (TEM) and optical microscopy, and gold colloids (5 nm in diameter) for merging several electron micrographs were added to the synthesis solutions of the mesoporous films. The dye molecules were incorporated into the pores during the evaporation-induced self-assembly of the material²⁰.

For the overlay of optical and electron microscopic images, we used Si₃N₄ membranes 30 nm in thickness supported by a small silicon wafer with a 500 μm × 500 μm window (Fig. 1b, c). The mesoporous film was spin-coated into the interior of the window.

Scanning electron micrographs (Supplementary Fig. 1) show that the polystyrene beads are embedded in the mesoporous film. We emphasize that no further sample preparation, such as ion milling, was needed for electron microscopy at low and high resolution or for the optical wide-field measurements. The whole membrane was mapped with successive white-light transmission images (Supplementary Fig. 2a; an enlargement is shown in Fig. 1d) before single-molecule fluorescence tracking. For the subsequent analysis by TEM, the whole membrane was first mapped at low resolution (Supplementary Fig. 2b), and then at higher magnification to distinguish between single polystyrene beads (Fig. 1e). In this map we were able to retrieve the same geometric arrangement of polystyrene beads as in the white-light images (Fig. 1f, g).

Figure 2 demonstrates the spatial correlation between the single-molecule trajectories (movie of 1,000 images, 200 ms per frame; Fig. 2b) and TEM (Fig. 2c). To overlay the trajectories on the TEM images, the positions of the polystyrene beads were determined from the same movie (red crosses in Fig. 2b). In the area of the tracked trajectories, 400 (20 × 20) TEM images were taken at ×40,000 magnification and were merged by using image cross-correlation and gold particle markers to obtain a map of an area of about 3.5 μm × 3.5 μm (Fig. 2c). From the geometric relationship of the polystyrene beads we fitted the scaling factor and rotating angle for overlaying the two images by the use of a least-square algorithm (Fig. 2d). In this procedure the bead positions in the TEM images were used as fixed references, and the wide-field images were scaled, rotated and translated during the fitting procedure. A more detailed description of the overlay procedure is given in Methods. As an example the bead positions and the deviations of the positions in the TEM and wide-field images of Fig. 2 are tabulated in Supplementary Table 1. We take the average deviation for the position of the polystyrene beads in both TEM and wide-field imaging as a measure for the accuracy of the overlay. It amounts to 26 nm for the overlaid images in Fig. 2d, calculated from the values in the last column of Supplementary Table 1. From the correlation of five different 3.5 μm × 3.5 μm TEM maps with the respective tracking data, we calculated the deviation of the bead positions in TEM and wide-field images to be 29 ± 13 nm (mean ± s.d.).

To show the orientation of the pores in the TEM images better, fast Fourier transformation (FFT) was applied to adjacent square regions of 133 nm × 133 nm (Fig. 2a). The results of the FFT are plotted as black lines. The orientation of each ‘director’ depicts the average orientation of the pores in the square region around it, and the line thickness is a measure for the intensity of the maxima in the FFT fit and thus for the degree of structural order in this region. In addition to the orientation of the channels, these directors give a good overview of the domain size and domain borders (Fig. 2a, c, d). The enlargement in Fig. 2e directly shows the channels and the

¹Department of Chemistry and Biochemistry and Center for NanoScience (CeNS), University of Munich, Butenandtstrasse 5-13 (E), D-81377 Munich, Germany.

*These authors contributed equally to this work.

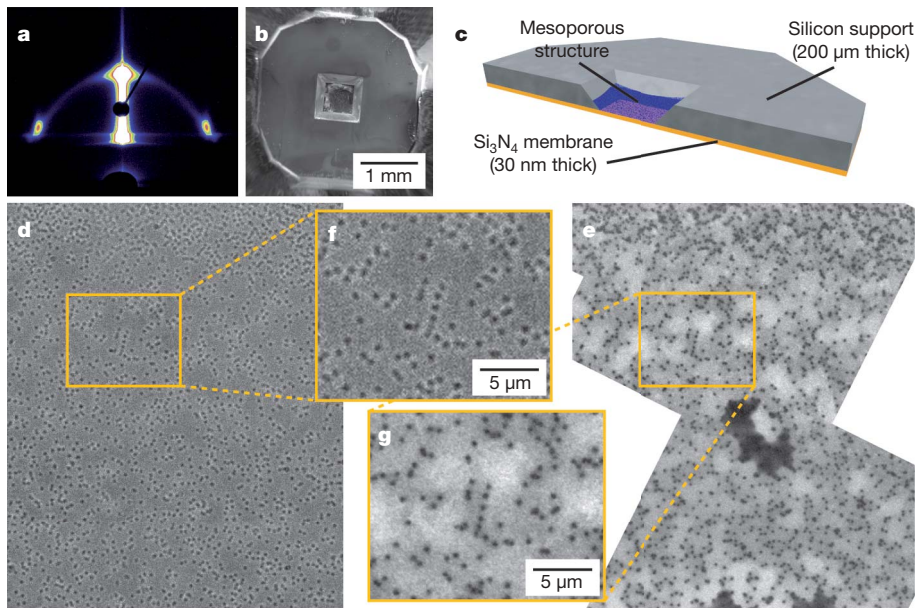


Figure 1 | Sample systems. **a**, A 2D-GISAXS pattern of the mesoporous film on a silicon wafer. **b**, Scanning electron micrograph of a coated Si_3N_4 membrane window on the silicon support. **c**, Diagram of a coated membrane. **d**, White-light transmission image of the region of interest. **e**, TEM image of the region of interest. **f**, **g**, The same characteristic formation of polystyrene beads shown by white-light transmission (**f**) and by TEM (**g**).

corresponding FFT directors, as well as the trajectories of the dye molecules along the channels.

The combination of the two techniques provides the first direct proof that the molecular diffusion pathway through the pore system correlates with the pore orientation of the two-dimensional hexagonal structure. In addition, the influence of specific structural features of the host on the diffusion behaviour of the guest molecules can be clearly seen. With this approach we can uncover, in unprecedented detail, how a single fluorescent dye molecule travels through linear or strongly curved sections of the hexagonal channel system in a thin film of mesoporous silica (as sketched in Fig. 3a, b), how it changes speed in the channel structure, and how it bounces off a domain boundary with a different channel orientation (Fig. 3c). Furthermore, we can show how molecular travel is stopped at a less ordered region (Fig. 3d), or how lateral motions between 'leaky' channels allow a molecule to

explore different parallel channels within an otherwise well-ordered periodic structure (Fig. 3e). Figure 4 depicts several examples of specific pore ordering, indicated by the FFT directors, in combination with the overlaid trajectories, showing the various structural features that are shown in Fig. 3. The positioning error for the single molecule trajectories is shown by the light blue boxes, which indicate the standard deviation of the fitted (x,y) positions. It is in the range of only 10–20 nm; the molecular positions can therefore be assigned to an ensemble of about five to ten parallel channels.

Figure 4a depicts a trajectory of a molecule that is following the porous system along different structural domains. The corresponding wide-field movie and the tracked trajectory of the single molecule overlaid with the TEM images are provided in Supplementary Movies 1 and 2. In this case the average deviation of the overlaid images is 34 nm (see Methods and Supplementary Information).

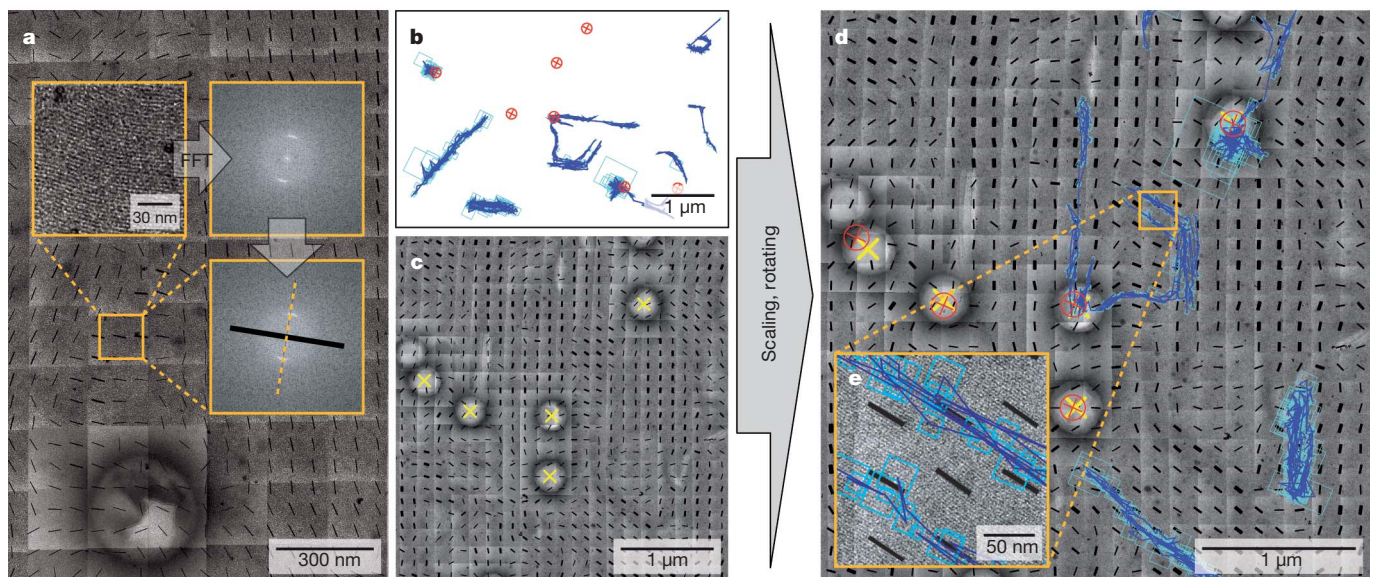


Figure 2 | Merging of the single-molecule trajectories and the TEM micrographs. **a**, The merged TEM map is redivided into equal-sized squares that are processed by FFT as shown in the insets. The direction of the channels is perpendicular to a straight line through the maxima. The thickness of the black directors, pointing along the pore direction, correlates with the structural quality. **b**, Diffusion pathways of single molecules through the pore system (blue trajectories) and positions of the polystyrene

beads (red crosses). **c**, The same area as in **b** is imaged by TEM, with lines indicating the direction of the channels (FFT directors) and yellow crosses marking the centres of the polystyrene beads. **d**, Final overlay of trajectories on TEM images; this was obtained by fitting to the best overlay of the polystyrene bead positions. **e**, Enlargement of a region in **d**, showing the trajectories running along the channels.

The molecule in Fig. 4a and Supplementary Movie 2 diffuses along linear pores in the middle part of the trajectory and follows the curvature on the right and on the left side. In addition, it turns at a domain boundary, as shown in more detail in Fig. 4b. The insets in the upper right corners of Fig. 4a, b show the different structural elements of this trajectory that were sketched in Fig. 3. To analyse the diffusion along this trajectory we projected the data points onto a manually defined backbone of the trajectory. Then we plotted the averaged mean-square displacement $\langle r^2 \rangle$ along the backbone as a function of time. The linear relation of $\langle r^2 \rangle$ with time was fitted in accordance with the Einstein–Smoluchowski equation for one-dimensional (1D) diffusion for the first few time lags²¹, resulting in a 1D diffusion coefficient D_{1D} of $(3.2 \pm 0.1) \times 10^{-2} \mu\text{m}^2 \text{s}^{-1}$. It is important to analyse the 1D diffusion along the backbone, because the r^2 in the curved region would otherwise tend towards smaller values for longer time lags.

Figure 4c shows another example of a molecule faithfully following the pores and mapping out specific elements of the host structure (see also Supplementary Movie 3). Here the average deviation of the overlay is 48 nm. In this case only one single bead and two pairs of closely neighbouring beads could be used for the overlay, which explains this relatively high value (see Methods). The molecule was blinking several times for intervals of up to 6.6 s, and the trajectory is therefore divided into 11 parts, with durations ranging from 0.6 s to 11.8 s, shown in different colours. The perfect overlay of the S-shaped trajectory on the pore system is shown well by the FFT directors. In Fig. 4d–f the specific regions marked with rectangular boxes in Fig. 4c are shown, and the insets sketch the different behaviours at specific regions of the trajectory (as in Fig. 3). Although the resolution of the optical microscope was not high enough to assign the position of a molecule to one specific channel, the width of the middle of this trajectory (magnified in Fig. 4d) shows that the molecule was moving in different straight parallel channels of the same domain. Especially interesting is the short element at the end of the yellow trajectory where the molecule makes a U-turn and diffuses back in a parallel track that is different from the original track, as shown at the left of Fig. 4d. On the basis of the spatial resolution of the optical pathways, we conclude that the molecule is diffusing in different parallel pores. At the left end of the trajectory in Fig. 4c the molecule diffuses in a well-ordered straight structure and bounces back repeatedly from an amorphous region having no apparent pore ordering, as shown in

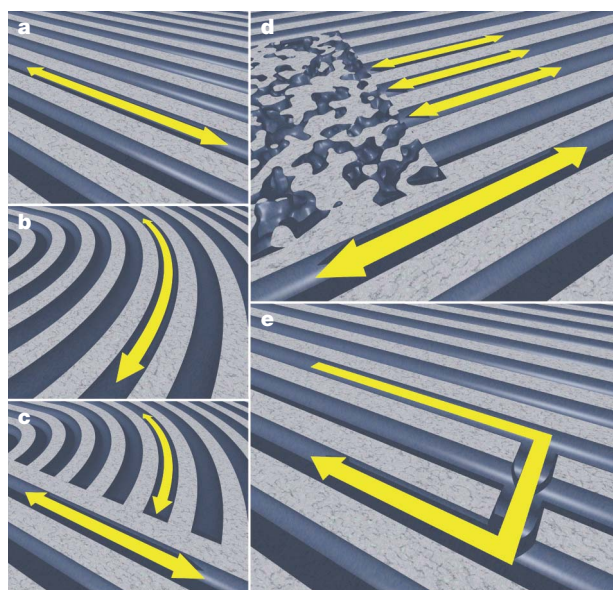


Figure 3 | Structural elements found in real two-dimensional hexagonal mesoporous silica film. **a, b**, Straight (**a**) and curved (**b**) segments. **c**, Domain boundaries forcing molecules to turn back. **d**, Molecular travel stopped at less ordered regions. **e**, Lateral motion between neighbouring channels.

Fig. 4e. At the right of Fig. 4c a domain boundary region is visible; this structure is shown in more detail in Fig. 4f. Here the molecule bounces back from the domain boundary with channels having different orientations, as sketched in Fig. 3c and in the inset. The orange lines in Fig. 4f are situated slightly above the region of linear channels. However, if the average deviation of the overlay of 48 nm is taken into account it is highly probable that the molecule was actually diffusing along the linear structure in the bottom region of the figure. Furthermore, one should keep in mind that we are sampling diffusion at discrete points in time and space. The connecting lines are just a method of visualizing the trajectories; they do not represent the molecules' exact path.

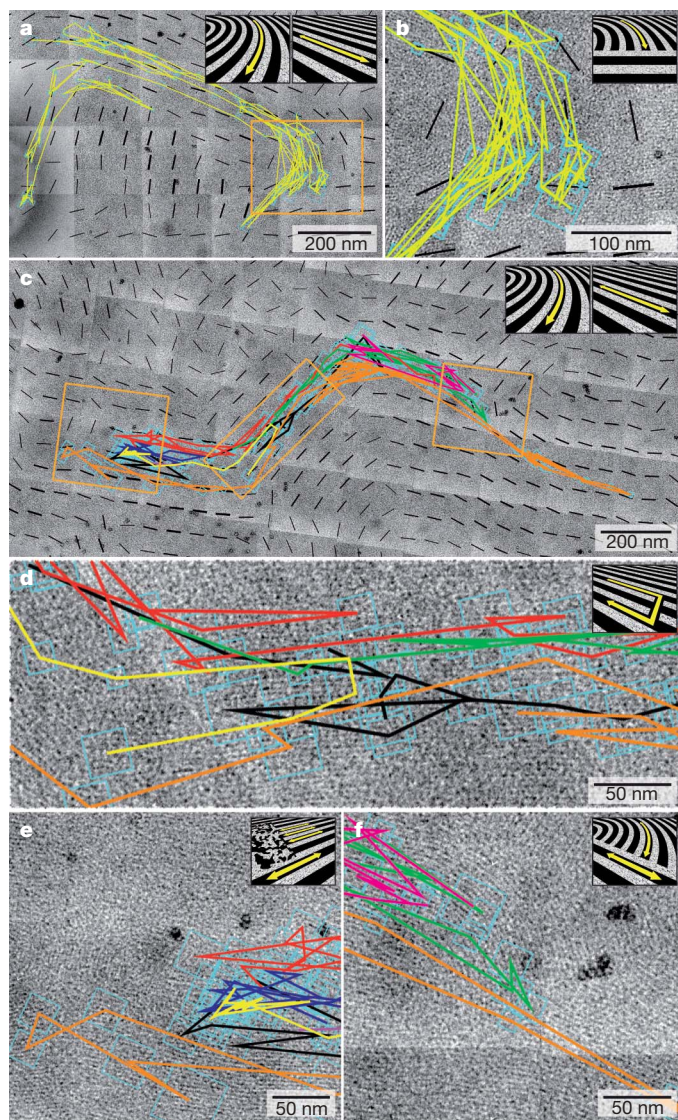


Figure 4 | Structural elements and molecular trajectories found in real two-dimensional hexagonal mesoporous silica film. **a**, Molecule exploring regions of parallel channels, strongly curved regions and domain boundaries. **b**, Magnified area from **a** showing the domain boundary at which the molecule turns back. **c**, Trajectory of another molecule, showing an S shape corresponding to the underlying channel structure. The trajectory is divided into several sections as a result of blinking of the fluorescent molecule; the sections are plotted in different colours. **d**, Lateral motions between 'leaky' channels (yellow trajectory). **e**, Area in which the molecular movement is stopped at a less ordered region. **f**, Forcing of the fluorescent molecule to turn back (green pathway) at a domain boundary. In all panels the light blue boxes depict the standard deviation of the fit to the single-molecule signals; that is, the positioning accuracy. Movies showing the diffusion of the single molecules in **a** and **c** are available as Supplementary Movies 1–3.

Projection of the trajectory shown in Fig. 4c onto its backbone and calculation of the average diffusion coefficient along the backbone gives $D_{1D} = (3.0 \pm 0.1) \times 10^{-2} \mu\text{m}^2 \text{s}^{-1}$. In addition, we calculated the following individual average diffusion coefficients for the parts of the trajectory showing no blinking for at least 20 frames: red (frames 1–33), $D_{1D} = (3.6 \pm 0.2) \times 10^{-2} \mu\text{m}^2 \text{s}^{-1}$; green (frames 37–82), $D_{1D} = (1.1 \pm 0.1) \times 10^{-2} \mu\text{m}^2 \text{s}^{-1}$; blue (frames 100–119), $D_{1D} = (1.0 \pm 0.1) \times 10^{-2} \mu\text{m}^2 \text{s}^{-1}$; yellow (frames 135–157), $D_{1D} = (2.0 \pm 0.1) \times 10^{-2} \mu\text{m}^2 \text{s}^{-1}$; orange (frames 176–244), $D_{1D} = (5.5 \pm 0.1) \times 10^{-2} \mu\text{m}^2 \text{s}^{-1}$; and violet (frames 308–328), $D_{1D} = (1.3 \pm 0.1) \times 10^{-2} \mu\text{m}^2 \text{s}^{-1}$. Parts of the trajectory with fewer than 20 points are drawn in black. The noticeable changes of the 'local' diffusion coefficient show that the diffusion behaviour of the molecules is strongly dependent on the surrounding pore structure. When the molecule is 'bouncing back' at an unstructured region, as in the dark blue part of the trajectory, D_{1D} is smaller than in regions where the molecule is diffusing along the trajectory (orange and red). On average the values are in the same range as the diffusion coefficient for the U-shaped trajectory shown in Fig. 4a and also many other trajectories observed in the same sample (not shown).

In this study we correlate directly the dynamic information from the diffusion trajectories of single guest molecules with the detailed structure of the porous host in regions up to $3.5 \mu\text{m} \times 3.5 \mu\text{m}$ in size. This approach reveals the nature of the real-space porous defect structure, as detected by the movement of fluorescent single molecules, containing linear or strongly curved sections of the hexagonal channel system, domain boundaries, boundaries between ordered and disordered sections, and leaky channels that permit lateral travel. We emphasize that our approach provides detailed information on the real defect structure of porous materials with high spatial resolution that cannot be obtained by scattering methods because of the intrinsic averaging effects. Similarly, we also obtain highly resolved dynamic information in real time that cannot be extracted from conventional diffusion techniques because of ensemble averaging. This new methodology is expected to provide detailed insights into the real structure and dynamics of other classes of porous materials and important host–guest systems, such as bioactive molecules in porous materials for drug delivery or reactants in porous catalysts.

METHODS SUMMARY

Synthesis. First, 2.08 g (0.01 mol) of tetraethyl orthosilicate (Sigma-Aldrich) were mixed with 3 g of 0.2 M HCl, 1.8 g of water and 7.9 g of ethanol and heated at 60°C for 1 h to accomplish acid-catalysed hydrolysis–condensation of the silica precursor. This solution was mixed with a second solution containing 600 mg of Brij 56 and 12.5 g of ethanol. Finally, 75 μl of this mixture were combined with 4 μl of a highly diluted TDI solution ($\sim 10^{-8} \text{ mol l}^{-1}$ in ethanol), 20 μl of a gold colloid solution (diameter 5 nm, concentration corresponding to $\sim 0.01\%$ HAuCl₄; Sigma-Aldrich), 15 μl of a polystyrene bead solution (Polybead microspheres, diameter $0.281 \pm 0.014 \mu\text{m}$, 2.6% solids (latex); Polysciences) and 40 μl of deionized water. The samples were prepared in dry air by spin-coating at 3,000 r.p.m. and then analysed as synthesized.

Ellipsometry. Ellipsometry measurements were performed on a Woollam ESM-300 ellipsometer.

TEM. TEM images were obtained with a JEOL 2011 transmission electron microscope operated at 200 kV by using the software-controlled mapping function of the charge-coupled device camera (model TVIPS F114).

2D-GISAXS. 2D-GISAXS was performed at beamline BW4 (HASYLAB, Hamburg).

Wide-field microscopy and single-particle tracking. Fluorescence images were recorded with a wide-field setup as described in Methods and in more detail in refs 9, 11. The fluorescent dye molecules were excited with a HeNe laser at 633 nm, and movies of 1,000 images were recorded to follow their diffusion. The examples presented here were measured with an exposure time of 200 ms per image. The individual molecule patterns are fitted by a gaussian function

$$f(x, y, A, w) = Ae^{-\left(\frac{x-x_0}{w}\right)^2} e^{-\left(\frac{y-y_0}{w}\right)^2}$$

with a positioning accuracy of down to 10 nm, where A and w are the amplitude and the width of the gaussian curve, respectively.

Full Methods and any associated references are available in the online version of the paper at www.nature.com/nature.

Received 13 August; accepted 18 October 2007.

- Beck, J. S. *et al.* A new family of mesoporous molecular sieves prepared with liquid-crystal templates. *J. Am. Chem. Soc.* **114**, 10834–10843 (1992).
- Sen, T., Tiddy, G. J. T., Casci, J. L. & Anderson, M. W. Synthesis and characterization of hierarchically ordered porous silica materials. *Chem. Mater.* **16**, 2044–2054 (2004).
- Zhao, D. *et al.* Triblock copolymer syntheses of mesoporous silica with periodic 50 to 300 angstrom pores. *Science* **279**, 548–552 (1998).
- Dag, Ö., Ozin, G. A., Yang, H., Reber, C. & Bussi ere, G. Photoluminescent silicon clusters in oriented hexagonal mesoporous silica film. *Adv. Mater.* **11**, 474–480 (1999).
- Davis, M. E. Ordered porous materials for emerging applications. *Nature* **417**, 813–821 (2002).
- Shen, J. L. *et al.* Photoluminescence sites on MCM-48. *Micropor. Mesopor. Mater.* **64**, 135–143 (2003).
- Yang, C.-M., Cho, A.-T., Pan, F.-M., Tsai, T.-G. & Chao, K.-J. Spin-on mesoporous silica films with ultralow dielectric constants, ordered pore structures, and hydrophobic surfaces. *Adv. Mater.* **13**, 1099–1102 (2001).
- Kukla, V. *et al.* NMR studies of single-file diffusion in unidimensional channel zeolites. *Science* **272**, 702–704 (1996).
- Hellriegel, C., Kirstein, J. & Br uchle, C. Tracking of single molecules as a powerful method to characterize diffusivity of organic species in mesoporous materials. *New J. Phys.* **7**, 23 (2005).
- Jung, C., Hellriegel, C., Michaelis, J. & Br uchle, C. Single-molecule traffic in mesoporous materials: translational, orientational, and spectral dynamics. *Adv. Mater.* **19**, 956–960 (2007).
- Kirstein, J. *et al.* Exploration of nanostructured channel systems with single-molecule probes. *Nature Mater.* **6**, 303–310 (2007).
- McCain, K. S., Hanley, D. C. & Harris, J. M. Single-molecule fluorescence trajectories for investigating molecular transport in thin silica sol-gel films. *Anal. Chem.* **75**, 4351–4359 (2003).
- Werley, C. A. & Moerner, W. E. Single-molecule nanoprobe explore defects in spin-grown crystals. *J. Phys. Chem. B* **110**, 18939–18944 (2006).
- Schmidt, T., Sch utz, G. J., Baumgartner, W., Gruber, H. J. & Schindler, H. Imaging of single molecule diffusion. *Proc. Natl Acad. Sci. USA* **93**, 2926–2929 (1996).
- Seisenberger, G. *et al.* Real-time single-molecule imaging of the infection pathway of an adeno-associated virus. *Science* **294**, 1929–1932 (2001).
- Roefsaers, M. B. J. *et al.* Spatially resolved observation of crystal-face-dependent catalysis by single turnover counting. *Nature* **439**, 572–575 (2006).
- Sakamoto, Y. *et al.* Direct imaging of the pores and cages of three-dimensional mesoporous materials. *Nature* **408**, 449–453 (2000).
- Holtrup, F. O. *et al.* Terrylenimides: new NIR fluorescent dyes. *Chem. Eur. J.* **3**, 219–225 (1997).
- Jung, C. *et al.* A new photostable terrylene diimide dye for applications in single molecule studies and membrane labeling. *J. Am. Chem. Soc.* **128**, 5283–5291 (2006).
- Brinker, C. J., Lu, Y., Sellinger, A. & Fan, H. Evaporation-induced self-assembly: nanostructures made easy. *Adv. Mater.* **11**, 579–585 (1999).
- Saxton, M. J. & Jacobson, K. Single-particle tracking: applications to membrane dynamics. *Annu. Rev. Biophys. Biomol. Struct.* **26**, 373–399 (1997).

Supplementary Information is linked to the online version of the paper at www.nature.com/nature.

Acknowledgements We thank K. M ullen for providing the TDI dye; Siltronic AG for the silicon wafers; the group of P. M uller-Buschbaum for the 2D-GISAXS measurements; and S. Schmidt and B. Platschek for assistance with electron microscopy. This work was funded by two Collaborative Research Centres ('Manipulation of matter at the nanometer length scale' and 'Dynamics and intermediates of molecular transformations') of the German Research Foundation (DFG) and by the Nanosystems Initiative Munich (NIM), as well as the Center for Integrated Protein Science Munich (CiPSM).

Author Information Reprints and permissions information is available at www.nature.com/reprints. Correspondence and requests for materials should be addressed to C.B. (christoph.braeuchle@cup.uni-muenchen.de) or T.B. (bein@lmu.de).

METHODS

Films for characterization by X-ray diffraction and ellipsometry. For X-ray diffraction and ellipsometry measurements, 200 μl of the final precursor solution were spin-coated on silicon wafers (28 mm \times 15 mm). The corresponding 2D-GISAXS pattern (Fig. 1a) shows a two-dimensional hexagonal order for the mesoporous silica, with the peaks corresponding to the d -spacings of $d(10) = 5.5$ nm and $d(01) = 5.9$ nm, respectively. The pore-to-pore distances are therefore $a(01) = 7.0$ nm (parallel to the substrate plane) and $a(10) = 6.5$ nm. The shrinkage of the pores normal to the substrate is 7%. The thickness determined by ellipsometry is about 100 nm.

Overlay of optical and electron microscopy images. For the preparation of the films, 50 μl of the final precursor solution were spin-coated on Si_3N_4 membranes 30 nm in thickness supported by a small silicon wafer with a 500 $\mu\text{m} \times 500$ μm window (Fig. 1b, c; PLANO; Wetzlar). The film on the central region of the supported membrane was thin enough for electron microscopy. The polystyrene beads and the gold nanoparticles were enclosed in the mesoporous film (Supplementary Fig. 1).

The wide-field microscopy setup was based on an Eclipse TE200 (Nikon) epifluorescence microscope with a high-numerical-aperture (NA) oil-immersion objective (Nikon Plan Apo 100 \times /1.40 NA oil). The molecules were excited at 633 nm with a HeNe gas laser (75 mW max. at 632.8 nm; Coherent) with an intensity of about 0.3 kW cm⁻², and their fluorescence was detected with a back-illuminated EM-CCD camera in frame transfer mode (iXon DV897, 512 pixels \times 512 pixels; Andor). Incident laser light was blocked by a dichroic mirror (640 nm cutoff; AHF) and a bandpass filter (730 nm/140 nm; AHF). Additional lenses ($f = 150$ mm, $f = 200$ mm, achromat; Thorlabs) in the detection pathway give an overall magnification of $\times 133$. This means that the side of one square pixel on the camera chip (16 μm) should represent 120 nm on the sample. By using the USAF test target (1951 Chromium positive; Melles Griot) this value was experimentally determined to 122 nm, which agrees well with the theoretical value. Because the films were much thinner than the focal depth of the microscope objective used (>1 μm), images contain data from molecules at all heights inside and on the surface of the sample. Series of 1,000 images were acquired with a temporal resolution of 200 ms per frame. In each movie frame, single molecules show up as bright spots. Because the Si_3N_4 membranes give a relatively high and inhomogeneous background signal, the background was subtracted frame-to-frame from the films before tracking of the molecules. Single-molecule trajectories were then built up by fitting the positions of the spots from frame to frame.

To overlay these trajectories on the TEM images, the positions of the polystyrene beads had to be determined from the same movie. For this purpose the laser shutter was closed for the last 240 frames of the movie and the polystyrene beads were imaged in transmission in white light (Supplementary Movie 1). Their positions were fitted in inverted images with the same gaussian fit routine as the single molecules (red crosses in Fig. 2b). Mean and standard deviations of the fitted positions were calculated and tabulated.

After optical microscopy the sample was analysed with TEM. Again, during the first step the whole membrane was mapped at low resolution (Supplementary Fig. 2b). The central region with the appropriate thickness was then mapped at a magnification high enough to distinguish single polystyrene beads (Fig. 1e). In this map we could retrieve the same geometric arrangement of polystyrene beads as in the white-light transmission images (Fig. 1f, g). In all, 400 (20 \times 20) images in the neighbourhood of the tracked trajectories were taken at $\times 40,000$ magnification and were merged by using image cross-correlation to obtain a map of an area of about 3.5 $\mu\text{m} \times 3.5$ μm . The centre positions of the polystyrene spheres in the TEM images were determined by fitting a circle on the outside margin of their patterns.

The overlay of the TEM and wide-field images was accomplished by fitting the best overlay of the polystyrene bead positions in the respective images by the use of a least-square algorithm (Fig. 2b–d). In this iterative process the sum of the squared deviations of the bead positions in TEM images and wide-field tracking data was minimized by scaling, rotating and translating the tracking data. As an example, Supplementary Table 1 shows the bead positions in the TEM images and in wide-field tracking data of Fig. 2 before and after the overlay procedure. In Fig. 2, the positions of four well-separated beads were used, yielding an average deviation of 26 nm after the overlay. The two beads at the left edge of the TEM image in Fig. 2c are too close to be resolved by optical microscopy. They are therefore not included in the overlay process. However, in some cases such pairs of closely neighbouring beads had to be used for the overlay to have a minimum of three anchor points for the overlay. In such cases, the individual positions of the closely neighbouring beads were determined in the TEM images. The centre position between the two beads was then correlated with the centre position of the single spot resulting from the two beads in the respective white-light transmission images, fitted by the gaussian function. For example, in Fig. 4d–f two such doubled beads had to be used for correlating tracking data and TEM images, which resulted in an average deviation of 48 nm.